

# Quantum Control for Time-dependent Noise by Inverse Geometric Optimization

Xiaodong Yang,<sup>1,2,3</sup> Xinfang Nie,<sup>4,1,2,3</sup> Tao Xin,<sup>1,2,3</sup> Dawei Lu,<sup>4,1,2,3,\*</sup> and Jun Li<sup>1,2,3,†</sup>

<sup>1</sup>Shenzhen Institute for Quantum Science and Engineering,  
Southern University of Science and Technology, Shenzhen, 518055, China

<sup>2</sup>International Quantum Academy, Shenzhen, 518055, China

<sup>3</sup>Guangdong Provincial Key Laboratory of Quantum Science and Engineering,  
Southern University of Science and Technology, Shenzhen, 518055, China

<sup>4</sup>Department of Physics, Southern University of Science and Technology, Shenzhen, 518055, China

Quantum systems are exceedingly difficult to engineer because they are sensitive to various types of noises. In particular, time-dependent noises are frequently encountered in experiments but how to overcome them remains a challenging problem. In this work, we extend and apply the recently proposed robust control technique of inverse geometric optimization to time-dependent noises by working it in the filter-function formalism. The basic idea is to parameterize the control filter function geometrically and minimize its overlap with the noise spectral density. This then effectively reduces the noise susceptibility of the controlled system evolution. We show that the proposed method can produce high-quality robust pulses for realizing desired quantum evolutions under realistic noise models, and thus will find practical applications for current physical platforms.

*Introduction.*—The ability to precisely manipulate quantum systems against noise is central to practical quantum information processing [1]. There have been developed a variety of robust quantum control methods, such as composite pulses [2–4], dynamical decoupling [5–7], sampling-based learning control [8, 9], geometric-formalism-based pulse control [10–15]. Many of these methods assume the considered noise to be quasi-static, i.e., slow enough compared to the operation time, which is however not always a valid noise model in reality. Actually, time-dependent noises are routinely encountered in experiments. For example,  $1/f$  type noise, which contains wide distribution of correlation times [16], is present in many solid-state qubit platforms such as superconducting qubits [17, 18] and semiconductor quantum dots [19, 20]. Therefore, in order to further enhance experimental control fidelities, it is of vital importance to develop robust quantum control for general time-dependent noises.

Attempts to address errors induced by time-dependent noises in quantum system engineering are challenging. Results to date suggest that conventional methods usually have their limitations. For example, composite pulses, originally designed to tackle static, systematic errors, were found to be robust to fluctuating noises up to as fast as around 10% of the Rabi frequency [21]. Dynamical decoupling can protect quantum coherence in a fluctuating environment, but it requires rapid and strong control modulation, which might be problematic to realize experimentally. Moreover, how to incorporate dynamical decoupling into the task of realizing arbitrary quantum operations is still not fully clear [22]. Optimal control provides a flexible and generically applicable approach, in which the requirements of pulse smoothness and robustness can be added as optimization constraints [23]. Usually, the control variables to be optimized are temporal pulse parameters such as amplitudes and phases. Alternatively, optimization can be done in the dynamical variable space with a geometric flavor, as proposed and developed in Refs. [10–15], yet only static errors have been considered therein.

In this work, we consider combing the geometric-based op-

timal control method with the filter function (FF) formalism [24–26] to overcome these limitations for the purpose of resisting time-dependent noises. FFs were originally introduced to evaluate operational infidelities under stationary stochastic noises, and have proven very useful in quantum control, especially for designing dynamical decoupling sequences [27–32]. Recently, there have been studies on incorporating FF into gradient-based optimal control [33]. Here, we take the geometric approach, that is, we first parameterize the controlled system evolution trajectory with dynamical variables, which corresponds to a parameterized filter function in the frequency domain, and then minimize the overlap of the filter function and the noise spectral density; see Fig. 1 for an illustration of the basic idea.

We give test examples of finding robust optimal control (ROC) pulses for producing target quantum gate and state transfer under realistic, experimentally relevant noise environments. It is found that our robust pulses outperform typical composite pulses in that their resultant FFs are suppressed at the characteristic frequencies of the considered noises, thus having much improved control fidelities. A separate section is devoted to treat the case of Markovian noise based directly on the Bloch equation, and the optimization results show that the  $T_1$  and  $T_2$  limit can be surpassed in the quantum state transfer task. Finally, discussions and implications are presented.

*Inverse geometric engineering.*—We consider a prototypical robust quantum control model, i.e., a resonantly controlled two-level system under time-dependent detuning noise and control amplitude noise. By convention, we parameterize the control field as  $\Omega(t)[\cos \phi(t), \sin \phi(t)]$  ( $t \in [0, T]$ ), with  $\Omega(t)$  ( $|\Omega(t)| \leq \Omega_{\max}$ ) being the pulsed Rabi frequency and  $\phi(t) \in [-\pi, \pi]$  the phase. Taking into account of noises, we have the following resonant frame Hamiltonian

$$H(t) = \Omega(1 + \epsilon_a(t)) \left[ \cos \phi \frac{\sigma_x}{2} + \sin \phi \frac{\sigma_y}{2} \right] + \epsilon_d(t) \frac{\sigma_z}{2}, \quad (1)$$

where  $\epsilon_a(t)$ ,  $\epsilon_d(t)$  represent fluctuating noises on control amplitude and detuning, respectively, and we introduce  $E_a(t) \equiv$

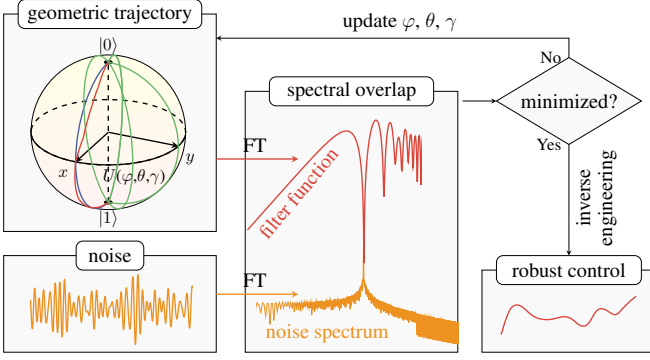


FIG. 1. Schematic diagram of the method of geometric- and FF-based pulse optimization for resisting time-dependent, stochastic noise. Since there exist many evolution trajectories realizing the same target but with different extent of noise filtering capabilities, the goal is hence to find a noise-resilient trajectory. For example, in the single-qubit case, the geometric trajectories generated by rectangular wave (blue line), composite pulse (green line), and a robust shaped pulse (red line) are plotted on the Bloch sphere for comparison, all implementing the same state transfer  $|0\rangle \rightarrow |1\rangle$ . Robust trajectory is found by minimizing the overlap of its associated control filter function with the noise spectral density. The pulse shape that generates this trajectory is then obtained through inverse engineering.

$\Omega[\cos\phi\sigma_x/2 + \sin\phi\sigma_y/2]$  and  $E_d \equiv \sigma_z/2$  as their corresponding noise operators. Physically, control amplitude noise is usually due to imperfect fabricated components, noisy electronics or varied fields [34], while detuning may originate from, e.g., random shifts in control driving frequency, or Overhauser effects on an electron spin by its surrounding nuclear spins [20]. In the following, we shall assume that  $\epsilon_a(t), \epsilon_d(t)$  are mutually independent stationary Gaussian processes with zero means. Under this assumption, each noise is fully characterized in terms of its own power spectral density  $S_\mu(\omega) = \int_{-\infty}^{\infty} dt e^{-i\omega t} \langle \epsilon_\mu(0)\epsilon_\mu(t) \rangle$ ,  $\mu \in \{a, d\}$ . For practical applications,  $S_\mu(\omega)$  will be determined from noise spectroscopy measurements in real experiments [35, 36].

Now, we briefly describe the inverse geometric optimization technique [10, 11]. The procedure starts with a parameterization of the noise-free evolution. Let  $U_0(t)$  be the solution to the time-dependent Schrödinger equation  $\dot{U}_0(t) = -iH_0(t)U_0(t)$ , where  $H_0(t)$  is as shown in Eq. (1) with  $\epsilon_a, \epsilon_d = 0$ . We parameterize  $U_0(t)$  based on ZYZ decomposition, that is, an arbitrary single-qubit unitary operator can be written as  $\exp(i\beta)R_z(\varphi)R_y(\theta)R_z(\gamma)$ , for some real numbers  $\beta, \varphi, \gamma \in [-\pi, \pi]$  and  $\theta \in [-\pi, \pi]$  [37]. In our problem here,  $\beta = 0$  because  $H_0$  is traceless. Hence, we have

$$U_0(t) = \begin{bmatrix} \cos(\theta/2)e^{-i\varphi/2}e^{-i\gamma/2} & -\sin(\theta/2)e^{-i\varphi/2}e^{i\gamma/2} \\ \sin(\theta/2)e^{i\varphi/2}e^{-i\gamma/2} & \cos(\theta/2)e^{i\varphi/2}e^{i\gamma/2} \end{bmatrix}.$$

As such, the Schrödinger equation is rewritten as

$$\dot{\theta} = \Omega \sin(\phi - \varphi), \quad (2a)$$

$$\dot{\varphi} = -\Omega \cos(\phi - \varphi) \cot \theta, \quad (2b)$$

$$\dot{\gamma} = \Omega \cos(\phi - \varphi) / \sin \theta. \quad (2c)$$

We perform optimization over these dynamical angular variables in order to find an evolution trajectory that has the property of dynamically correcting errors on itself. In this geometric formulation of the control problem, the optimization objective consists of control target, robustness requirement, boundary conditions and certain practical considerations such as bounded control amplitude, all expressed in terms of  $\theta, \varphi$  and  $\gamma$ . Once a robust evolution trajectory specified by the three angular variables is obtained, we can determine the control field by evaluating the inversion of Eq. (2), i.e.,  $\Omega = \sqrt{\dot{\theta}^2 + \dot{\gamma}^2 \sin^2 \theta}$ ,  $\phi = \arcsin(\dot{\theta}/\Omega) + \varphi$ .

*Quantum gate and quantum state transfer.*—We first consider the control target of implementing a desired quantum gate or quantum state transfer. The key step is to effect the transformation operator to the toggling frame defined by  $U_{\epsilon_a, \epsilon_d}(t) = U_0(t)U_{\text{tog}}(t)$ , where  $U_{\epsilon_a, \epsilon_d}(t)$  represents the propagator in the presence of the noises. Through Dyson perturbative expansion [38], there is  $U_{\text{tog}}(t) = \mathbb{1} - \sum_{\mu=a,d} [i \int_0^t dt_1 \epsilon_\mu(t_1) \tilde{E}_\mu(t_1) + \int_0^t dt_1 \int_0^{t_1} dt_2 \epsilon_\mu(t_1) \epsilon_\mu(t_2) \tilde{E}_\mu(t_1) \tilde{E}_\mu(t_2) + \dots]$  with  $\mathbb{1}$  the identity operator and  $\tilde{E}_\mu(t) = U_0^\dagger(t)E_\mu U_0(t)$ ,  $\mu \in \{a, d\}$ . Substitute into the parameterized  $U_0(t)$ , we obtain  $\tilde{E}_{a,x}(t) = [\dot{\theta} \sin \gamma + (\dot{\gamma} \sin 2\theta \cos \gamma)/2]\sigma_x/2$ ,  $\tilde{E}_{a,y}(t) = [\dot{\theta} \cos \gamma - (\dot{\gamma} \sin 2\theta \sin \gamma)/2]\sigma_y/2$ ,  $\tilde{E}_{a,z}(t) = (\dot{\gamma} \sin^2 \theta)\sigma_z/2$ ;  $\tilde{E}_{d,x}(t) = (-\sin \theta \cos \gamma)\sigma_x/2$ ,  $\tilde{E}_{d,y}(t) = (\sin \theta \sin \gamma)\sigma_y/2$ ,  $\tilde{E}_{d,z}(t) = (\cos \theta)\sigma_z/2$ . These formulas are then to be substituted into the Dyson series to evaluate the error terms.

For the quantum gate problem, we are given a target gate  $\bar{U}$  and intend to find a robust implementing pulse. Suppose that the ideal evolution at time  $T$  satisfies  $U_0(T) = \bar{U}$ , then for a single realization of  $\epsilon_a(t)$  and  $\epsilon_d(t)$ , the gate fidelity reads  $F = |\text{Tr}(\bar{U}^\dagger U_{\epsilon_a, \epsilon_d}(T))|^2 / 4 = |\text{Tr}(U_{\text{tog}}(T))|^2 / 4$ . Taking the ensemble average of the noises and transferring to the frequency domain, the average gate infidelity defined by  $\mathcal{F}_{\text{avg}} = 1 - \langle F \rangle$  can be estimated to the second order approximation by the filter-function formalism [39, 40]

$$\mathcal{F}_{\text{avg}} \approx \frac{1}{2\pi} \sum_{\substack{\mu=a,d \\ \alpha=x,y,z}} \int_{-\infty}^{\infty} \frac{d\omega}{\omega^2} S_\mu(\omega) |R_{\mu,\alpha}(\omega)|^2, \quad (3)$$

in which  $R_{\mu,\alpha}(\omega) = -i\omega \int_0^T dt \text{Tr}[\tilde{E}_{\mu,\alpha}(t)\sigma_\alpha/2]e^{i\omega t}$ , and  $\sum_\alpha |R_{d,\alpha}(\omega)|^2/\omega^2, \sum_\alpha |R_{a,\alpha}(\omega)|^2/(\omega^2\Omega_{\text{max}}^2)$  are the so called filter functions. This formula provides a simple quantitative means to evaluate the performance of a control protocol in the presence of time-dependent noises. It is thus natural to take  $\mathcal{F}_{\text{avg}}$  as our objective function. As a concrete example, we consider implementing a  $\pi$  rotational gate  $\bar{U} = \exp(-i\pi\sigma_y/2)$ . For this problem, at  $t = 0$ ,  $U_0(0)$  equals to the identity, corresponding to the initial conditions  $\theta(0) = 0$  and  $\varphi(0) = -\gamma(0)$  (value not specified). The ending point conditions are  $\theta(T) = \pi$  and  $\varphi(T) = \gamma(T)$ . The latter can be rewritten as a constraint for  $\theta$  and  $\gamma$  by noting that from Eqs. (2b) and (2c) there is  $\dot{\varphi} = -\dot{\gamma} \cos(\theta)$ , hence one requires

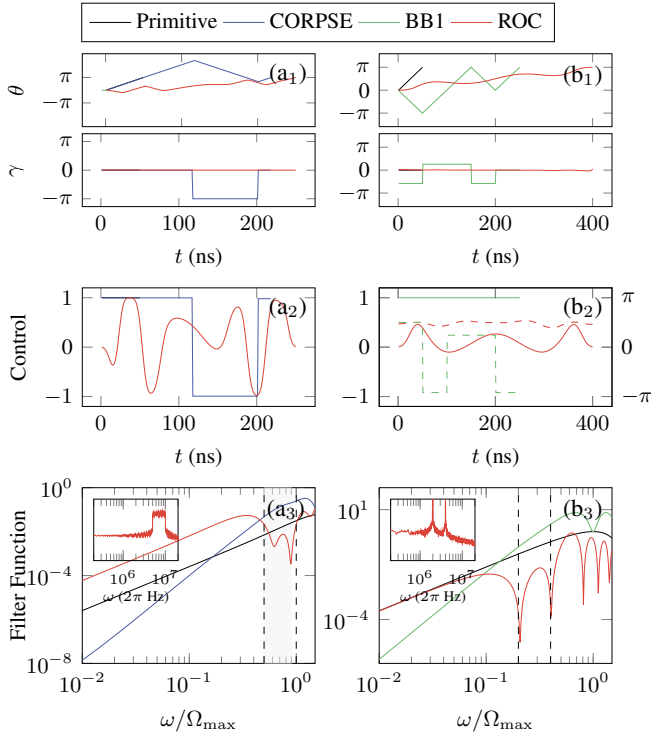


FIG. 2. Geometric trajectories, control waveforms, FFs and noise spectra of different sequences for realizing a  $\pi$  rotational gate subject to time-dependent noise. (a<sub>1</sub>)–(a<sub>3</sub>) For detuning noise, the noise strength is set as  $\sqrt{\langle \epsilon_d^2(0) \rangle} = 0.03\Omega_{\max}$  with  $\Omega_{\max}/(2\pi) = 10^7$  Hz, and the noise spectrum is ohmic. (b<sub>1</sub>)–(b<sub>3</sub>) For amplitude noise, its strength is  $\sqrt{\langle \epsilon_a^2(0) \rangle} = 0.03$ , and the noise spectrum is two Lorentzian peaks added on top of  $1/f$  background ( $\lambda_1 = \lambda_2 = 100$  Hz,  $\kappa = 1, A_1 = A_2 = 1, B = 0.05$ ). The solid lines in (a<sub>2</sub>) and (b<sub>2</sub>) represent the pulse amplitudes in the unit of  $\Omega_{\max}$ , and the dashed lines in (b<sub>2</sub>) are the pulse phases depicted by axis on the right. It can be seen that ROC FFs are suppressed at the characteristic frequencies, implying better noise filtering capability. Meanwhile, ROC control waveforms and geometric trajectories are much smoother.

the condition  $\gamma(0) + \gamma(T) + \int_0^T \dot{\gamma} \cos \theta dt = 0$  to be satisfied. With the objective function and all the constraints, we search ROC pulses using the gradient-based algorithm [41]; see details in Supplemental Material [40].

For the quantum state transfer problem, without loss of generality, we suppose the initial state to be  $|0\rangle$ . The target is an arbitrary state  $|\bar{\psi}\rangle$  on the Bloch sphere. For one realization of the noise  $\epsilon_a(t)$  and  $\epsilon_d(t)$ , the state transfer fidelity reads  $F = |\langle \bar{\psi} | U_{\epsilon_a, \epsilon_d}(T) | 0 \rangle|^2$ . Suppose the ideal evolution  $U_0(T)$  implements the desired state transfer. Again, we turn into the toggling frame and get  $F = |\langle 0 | U_{\log}(T) | 0 \rangle|^2$ . Substitute into the perturbative expansion of  $U_{\log}(T)$ , and take ensemble average of the noise Hamiltonian, it can be derived that the average state infidelity is

$$\mathcal{F}_{\text{avg}} \approx \sum_{\substack{\mu=\alpha, d \\ \alpha=x, y, z}} \frac{1}{2\pi} \int_{-\infty}^{\infty} \frac{d\omega}{\omega^2} S_{\mu}(\omega) |P_{\mu, \alpha}(\omega)|^2, \quad (4)$$

where we define  $P_{\mu, \alpha} = -i\omega \int_0^T dt \langle 0 | \tilde{E}_{\mu, \alpha}(t) | 1 \rangle e^{i\omega t}$ , and  $\sum_{\alpha} |P_{d, \alpha}(\omega)|^2 / \omega^2, \sum_{\alpha} |P_{a, \alpha}(\omega)|^2 / (\omega^2 \Omega_{\max}^2)$  are the filter functions [40]. Concretely, we consider preparing target state  $|\bar{\psi}\rangle = |1\rangle$  starting from  $|0\rangle$ . This converts to the conditions  $\theta(0) = 0, \theta(T) = \pi, \varphi(0) = \varphi(T) = 0$ , and no requirement of  $\gamma$  is involved. Moreover, the relation between  $\theta$  and  $\gamma$ , namely  $\dot{\varphi} = -\dot{\gamma} \cos(\theta)$ , requires the condition  $\int_0^T \dot{\gamma} \cos \theta dt = 0$  to be satisfied. The optimization procedure is the same as that described in the gate problem.

As demonstration, we show the numerical simulation results of implementing a  $\pi$  rotational gate under realistic detuning or amplitude noise, as shown in in Fig. 2. We compare performances between primitive, typical composite pulses and robust optimal control pulses, for the same given noise spectrum. The primitive pulse is the elementary rectangular pulse of maximum Rabi frequency  $\Omega_{\max}$ , which corresponds to the time-minimal control  $t_{\min} = 1/(2\Omega_{\max})$ . For detuning noise, as shown in Figs. 2(a<sub>1</sub>)–2(a<sub>3</sub>), we consider ohmic spectrum with sharp cut-offs, i.e.,  $S_d(\omega) \propto \omega, \omega \in [\omega_{lc}, \omega_{uc}]$ , which describes a spin suffering bosonic environment [42]. The composite pulse we chosen is CORPSE [43], which is robust to detuning error to the first order. For amplitude noise, as shown in Figs. 2(b<sub>1</sub>)–2(b<sub>3</sub>), we examine a noise spectrum of several Lorentzian peaks added on top of a broad  $1/f^{\kappa}$  background  $S_a(\omega) \propto \sum_k A_k / (\lambda_k^2 + (\omega - \omega_{0,k})^2) + B/\omega^{\kappa}$ , which describes the random fluctuations in superconducting flux terms [44]. The composite pulse tested for this case is BB1 [43], which is robust to amplitude error to the second order. It can be seen that in each test example, the ROC filter function has sharp dips at the central frequencies of the imported noise spectrum, hence their frequency overlap is significantly suppressed; see Figs. 2(a<sub>3</sub>) and 2(b<sub>3</sub>). This feature implies that ROC has better performance in mitigating time-dependent noises. We can verify this conclusion by computing their fidelities as follows. We calculate a single instance of noise perturbed evolution operator  $U_{\epsilon_a}(T)$  and a single value for fidelity, and then take average over  $N = 150$  noise realizations. For detuning noise with ohmic spectrum centered in the range  $[0.5\Omega_{\max}, \Omega_{\max}]$ , as shown in the insert of Fig. 2(a<sub>3</sub>), we obtain  $\mathcal{F}_{\text{avg}}^{\text{ROC}} = 4 \times 10^{-4}$ , while  $\mathcal{F}_{\text{avg}}^{\text{Primitive}} = 1 \times 10^{-3}$  and  $\mathcal{F}_{\text{avg}}^{\text{CORPSE}} = 9 \times 10^{-3}$ . This result is consist with the conclusion that composite pulses are only robust to fluctuating noises up to as fast as around 10% of the Rabi frequency [21], yet our ROC pulse can still function for high-frequency noise. For amplitude noise with Lorentzian peaks centered at  $0.2\Omega_{\max}$  and  $0.4\Omega_{\max}$  (see the insert of Fig. 2(b<sub>3</sub>)), we obtain  $\mathcal{F}_{\text{avg}}^{\text{Primitive}} = 2 \times 10^{-3}$  and  $\mathcal{F}_{\text{avg}}^{\text{BB1}} = 8 \times 10^{-3}$ , while our ROC pulse can decrease the infidelity to  $\mathcal{F}_{\text{avg}}^{\text{ROC}} = 4 \times 10^{-6}$ . Another benefit of ROC pulse is that its shape can be made much smoother than CORPSE and BB1; see Figs. 2(a<sub>2</sub>) and 2(b<sub>2</sub>). This is particularly favorable for experiments, as real pulse generators have limited bandwidths. Accordingly, ROC produces smoother geometric evolution trajectories, as shown in Figs. 2(a<sub>1</sub>) and 2(b<sub>1</sub>).

More simulation results for state transfer from  $|0\rangle$  to  $|1\rangle$ ,

for the case when detuning and amplitude noise are simultaneously present, for other types of realistic noise models, and for varied characteristic frequency positions of the tested noise spectra are all put in the Supplemental Material [40]. These results reveal that, in general, ROC pulses offer fidelity improvement for almost an order of magnitude compared with composite pulses and primitive pulse, and meanwhile featuring smooth pulse shapes and geometric trajectories.

*Resistance of  $T_1, T_2$  relaxation.*— When noises vary fast such that the Markovian approximation is valid, the controlled system dynamics can be described by the Bloch equation [45]  $\dot{x} = (H_0(t) + \gamma_1 R_{T_1} + \gamma_2 R_{T_2})x$ , where  $x \equiv (1/2, x_1, x_2, x_3)^T$  is the vectorized representation of the system density matrix  $\rho = \mathbb{1}/2 + x_1\sigma_x + x_2\sigma_y + x_3\sigma_z$  ( $x_1^2 + x_2^2 + x_3^2 \leq 1/4$ ),  $H_0(t)$  is the control Hamiltonian,  $\gamma_{1,2} = 1/T_{1,2}$  are relaxation rates and

$$R_{T_1} = \begin{pmatrix} 0 & 0 & 0 & 0 \\ 0 & 0 & 0 & 0 \\ 0 & 0 & 0 & 0 \\ 2 & 0 & 0 & -1 \end{pmatrix}, R_{T_2} = \begin{pmatrix} 0 & 0 & 0 & 0 \\ 0 & -1 & 0 & 0 \\ 0 & 0 & -1 & 0 \\ 0 & 0 & 0 & 0 \end{pmatrix} \quad (5)$$

are their corresponding operators. Relaxation is an irreversible process, hence it is usually thought that the best strategy to alleviate effects of relaxation is to make the operation time as small as possible. Therefore, the primitive pulse sets a fundament limit hard to surpass by other pulses [11]. Here, we study this issue using inverse geometric optimization, which works as follows. We first parameterize the relaxation-free evolution with extended three-dimensional rotations  $R_z(\delta), R_y(\eta)$  and  $R_z(\xi)$ , namely  $V_0(t) = \begin{pmatrix} 1 & 0 \\ 0 & R_z(\delta)R_y(\eta)R_z(\xi) \end{pmatrix}$  with  $\delta, \xi \in [-\pi, \pi], \eta \in [0, \pi]$  [40]. Thus, the Bloch equation is rewritten as

$$\dot{\xi} = \Omega \cos(\phi - \delta) / \sin \eta, \quad (6a)$$

$$\dot{\eta} = \Omega \sin(\phi - \delta), \quad (6b)$$

$$\dot{\delta} = -\Omega \cos(\phi - \delta) / \tan \eta. \quad (6c)$$

The actual evolution is then transformed to the toggling frame for conveniently displaying the perturbation effects due to  $T_1$  and  $T_2$  relaxation, i.e.,  $V_{T_1, T_2}(t) = V_0(t)V_{\text{tog}}(t) \approx V_0(t)(\mathbb{1}_4 + \sum_k \int_0^t dt_1 \gamma_k \tilde{R}_{T_k}(t_1) + \dots)$ , where  $\mathbb{1}_4$  is the 4-dimensional identity,  $\tilde{R}_{T_k}(t) = V_0^\dagger(t)R_{T_k}V_0(t)$ .

Take the quantum state transfer problem as an example. Starting from state  $x(0)$ , the Euclidean distance between the actual state and the target state  $\bar{x}$ , defined by  $\mathcal{F} = |\bar{x} - V_{T_1, T_2}(T)x(0)|^2$ , can be expressed in terms of the angular variables as follows [40]

$$\mathcal{F} \approx \int_0^T dt [\gamma_1^2 (\cos \eta - 2)^2 + \gamma_2^2 \sin^2 \eta] / 4. \quad (7)$$

As a concrete example, we consider quantum state transfer from the north pole  $x(0) = [1/2, 0, 0, 1/2]^T$  to the south pole  $\bar{x} = [1/2, 0, 0, -1/2]^T$ . This gives the constraint conditions  $\eta(0) = 0, \eta(T) = \pi$  and we set  $\delta(0) = \delta(T) = 0$ ,

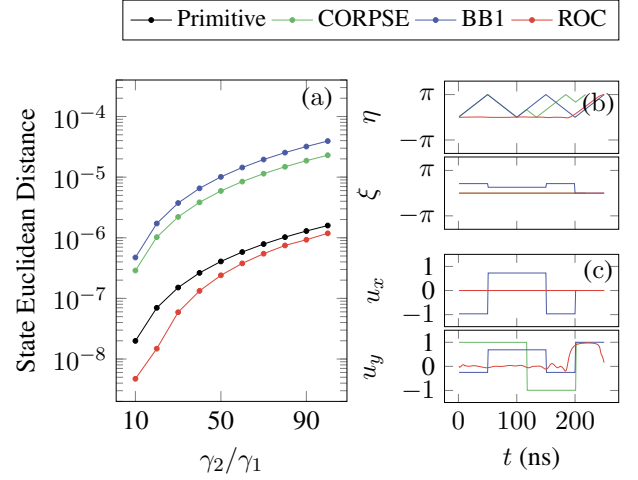


FIG. 3. Performance comparison of different sequences for realizing state transfer from the north pole to the south pole subject to both transverse and longitudinal relaxation. (a) State Euclidean distance vs different relaxation parameters, where we set  $\gamma_1 = 10^3 \text{ s}^{-1}$ . Specifically, we show geometric trajectories and control waveforms (in the unit of  $\Omega_{\text{max}}$ ) for the case of  $\gamma_2/\gamma_1 = 10$  in (b) and (c), respectively.

while no requirement of  $\xi$  is involved. Besides, from Eqs. (6a) and (6c) we have  $\dot{\delta} = -\dot{\xi} \cos \eta$ , thus the condition  $\int_0^T \dot{\xi} \cos \eta dt = 0$  should be satisfied. In our optimization, we also use the gradient-based algorithm to search robust ROC pulses. Results are summarized in Fig. 3, where we consider solid-state spin defect system with  $\Omega_{\text{max}}/(2\pi) = 10^7 \text{ Hz}$ , and the relaxation parameters are typically chosen as  $\gamma_1 = 10^3 \text{ s}^{-1}, \gamma_2/\gamma_1 = 10 \sim 100$  [46]. From Fig. 3(a), we find that typical composite pulses, including CORPSE and BB1, can not resist relaxation, as they result in much larger errors compared with the primitive pulse. On the other hand, ROC pulses can improve up to four times compared with primitive pulse for all the tested relaxation parameters. Meanwhile, the geometric trajectories and control waveforms for ROC pulses are smoother, as shown in Figs. 3(b) and 3(c), respectively.

*Discussion and outlook.*—The task of mitigating time-dependent noises is generally considered to be a thorny challenge and a long-term objective of quantum system engineering. The robust control method presented here has a critical advantage of flexibility as it is effective for a wide variety of noise environments, which is hence particularly applicable in reality since real experiments often involve complicated noise spectrum. Moreover, in the Markovian limit, the method is also effective in improving the state transfer fidelity against transverse and longitudinal relaxation effects. We hope the control examples tested here or other possible applications can soon find their experimental verifications.

For future work, we can combine inverse geometric engineering with other robust optimal control methods. For example, the technique developed in Ref. [47], which expresses Dyson perturbative terms based on Van Loan's integral ex-



pression, provides a rather convenient means to evaluate the perturbative impacts of the noises. We can also apply analytic expression of the filter function derivatives [33] to further improve the performance of our method, or attempt to derive exact analytical control fields [48, 49]. In addition, the method presented here can be easily extended to handle other robust quantum control tasks, such as quantum sensing under time-dependent background noises [50].

*Acknowledgments.* We thank Ze Wu for helpful discussions. This work was supported by the National Natural Science Foundation of China (1212200199, 11975117, 92065111, 12075110, 11905099, 11875159, 11905111, and U1801661), National Key Research and Development Program of China (2019YFA0308100), Guangdong Basic and Applied Basic Research Foundation (2019A1515011383 and 2021B1515020070), Guangdong Provincial Key Laboratory (2019B121203002), Guangdong International Collaboration Program (2020A0505100001), Shenzhen Science and Technology Program (RCYX20200714114522109 and KQTD20200820113010023), China Postdoctoral Science Foundation (2021M691445), Science, Technology and Innovation Commission of Shenzhen Municipality (ZDSYS20190902092905285, KQTD20190929173815000 and JCYJ20200109140803865), and Pengcheng Scholars, Guangdong Innovative and Entrepreneurial Research Team Program (2019ZT08C044).

---

\* ludw@sustech.edu.cn

† lij3@sustech.edu.cn

- [1] D. Suter and G. A. Álvarez, Colloquium: Protecting quantum information against environmental noise, *Rev. Mod. Phys.* **88**, 041001 (2016).
- [2] M. H. Levitt, Composite pulses, *Prog. Nucl. Magn. Reson. Spectrosc.* **18**, 61 (1986).
- [3] H. K. Cummins, G. Llewellyn, and J. A. Jones, Tackling systematic errors in quantum logic gates with composite rotations, *Phys. Rev. A* **67**, 042308 (2003).
- [4] K. R. Brown, A. W. Harrow, and I. L. Chuang, Arbitrarily accurate composite pulse sequences, *Phys. Rev. A* **70**, 052318 (2004).
- [5] L. Viola, E. Knill, and S. Lloyd, Dynamical Decoupling of Open Quantum Systems, *Phys. Rev. Lett.* **82**, 2417 (1999).
- [6] L. Viola and E. Knill, Robust Dynamical Decoupling of Quantum Systems with Bounded Controls, *Phys. Rev. Lett.* **90**, 037901 (2003).
- [7] A. M. Souza, G. A. Álvarez, and D. Suter, Robust dynamical decoupling, *Phil. Trans. R. Soc. A* **370**, 4748 (2012).
- [8] C. Chen, D. Dong, R. Long, I. R. Petersen, and H. A. Rabitz, Sampling-based learning control of inhomogeneous quantum ensembles, *Phys. Rev. A* **89**, 023402 (2014).
- [9] D. Dong, M. A. Mabrok, I. R. Petersen, B. Qi, C. Chen, and H. Rabitz, Sampling-based learning control for quantum systems with uncertainties, *IEEE Trans. Control Syst. Technol.* **23**, 2155 (2015).
- [10] D. Daems, A. Ruschhaupt, D. Sugny, and S. Guérin, Robust Quantum Control by a Single-Shot Shaped Pulse, *Phys. Rev. Lett.* **111**, 050404 (2013).
- [11] G. Dridi, K. Liu, and S. Guérin, Optimal Robust Quantum Control by Inverse Geometric Optimization, *Phys. Rev. Lett.* **125**, 250403 (2020).
- [12] E. Barnes, X. Wang, and S. D. Sarma, Robust quantum control using smooth pulses and topological winding, *Sci. Rep.* **5**, 12685 (2015).
- [13] J. Zeng, C. H. Yang, A. S. Dzurak, and E. Barnes, Geometric formalism for constructing arbitrary single-qubit dynamically corrected gates, *Phys. Rev. A* **99**, 052321 (2019).
- [14] D. Buterakos, S. Das Sarma, and E. Barnes, Geometrical Formalism for Dynamically Corrected Gates in Multiqubit Systems, *PRX Quantum* **2**, 010341 (2021).
- [15] U. Güngördü and J. P. Kestner, Analytically parametrized solutions for robust quantum control using smooth pulses, *Phys. Rev. A* **100**, 062310 (2019).
- [16] E. Paladino, Y. M. Galperin, G. Falci, and B. L. Altshuler,  $1/f$  noise: Implications for solid-state quantum information, *Rev. Mod. Phys.* **86**, 361 (2014).
- [17] J. Clarke and F. K. Wilhelm, Superconducting quantum bits, *Nature* **453**, 1031 (2008).
- [18] P. Krantz, M. Kjaergaard, F. Yan, T. P. Orlando, S. Gustavsson, and W. D. Oliver, A quantum engineer's guide to superconducting qubits, *Appl. Phys. Rev.* **6**, 021318 (2019).
- [19] T. D. Ladd, F. Jelezko, R. Laflamme, Y. Nakamura, C. Monroe, and J. L. O'Brien, Quantum computers, *Nature* **464**, 45 (2010).
- [20] F. K. Malinowski, F. Martins, L. Cywiński, M. S. Rudner, P. D. Nissen, S. Fallahi, G. C. Gardner, M. J. Manfra, C. M. Marcus, and F. Kuemmeth, Spectrum of the Nuclear Environment for GaAs Spin Qubits, *Phys. Rev. Lett.* **118**, 177702 (2017).
- [21] C. Kabytayev, T. J. Green, K. Khodjasteh, M. J. Biercuk, L. Viola, and K. R. Brown, Robustness of composite pulses to time-dependent control noise, *Phys. Rev. A* **90**, 012316 (2014).
- [22] J. Zhang, A. M. Souza, F. D. Brandao, and D. Suter, Protected quantum computing: Interleaving gate operations with dynamical decoupling sequences, *Phys. Rev. Lett.* **112**, 050502 (2014).
- [23] J. Werschnik and E. K. U. Gross, Quantum optimal control theory, *J. Phys. B: At. Mol. Opt. Phys.* **40**, R175 (2007).
- [24] J. M. Martinis, S. Nam, J. Aumentado, K. M. Lang, and C. Urbina, Decoherence of a superconducting qubit due to bias noise, *Phys. Rev. B* **67**, 094510 (2003).
- [25] A. G. Kofman and G. Kurizki, Unified theory of dynamically suppressed qubit decoherence in thermal baths, *Phys. Rev. Lett.* **93**, 130406 (2004).
- [26] G. S. Uhrig, Keeping a quantum bit alive by optimized  $\pi$ -pulse sequences, *Phys. Rev. Lett.* **98**, 100504 (2007).
- [27] G. Gordon, G. Kurizki, and D. A. Lidar, Optimal Dynamical Decoherence Control of a Qubit, *Phys. Rev. Lett.* **101**, 010403 (2008).
- [28] M. J. Biercuk, H. Uys, A. P. VanDevender, N. Shiga, W. M. Itano, and J. J. Bollinger, Optimized dynamical decoupling in a model quantum memory, *Nature* **458**, 996 (2009).
- [29] H. Uys, M. J. Biercuk, and J. J. Bollinger, Optimized Noise Filtration through Dynamical Decoupling, *Phys. Rev. Lett.* **103**, 040501 (2009).
- [30] J. Clausen, G. Bensky, and G. Kurizki, Bath-Optimized Minimal-Energy Protection of Quantum Operations from Decoherence, *Phys. Rev. Lett.* **104**, 040401 (2010).
- [31] C. Kabytayev, *Quantum control for time-dependent noise* (Ph.D. Thesis, Georgia Institute of Technology, 2015).
- [32] M. Biercuk, A. Doherty, and H. Uys, Dynamical decoupling sequence construction as a filter-design problem, *J. Phys. B: At. Mol. Opt. Phys.* **44**, 154002 (2011).
- [33] I. N. M. Le, J. D. Teske, T. Hangleiter, P. Cerfontaine, and H. Bluhm, Analytic filter-function derivatives for quantum op-

- timal control, *Phys. Rev. Applied* **17**, 024006 (2022).
- [34] C. Ferrie and O. Moussa, Robust and efficient in situ quantum control, *Phys. Rev. A* **91**, 052306 (2015).
- [35] T. Yuge, S. Sasaki, and Y. Hirayama, Measurement of the noise spectrum using a multiple-pulse sequence, *Phys. Rev. Lett.* **107**, 170504 (2011).
- [36] G. A. Álvarez and D. Suter, Measuring the spectrum of colored noise by dynamical decoupling, *Phys. Rev. Lett.* **107**, 230501 (2011).
- [37] M. A. Nielsen and I. L. Chuang, *Quantum Computation and Quantum Information* (Cambridge University Press, Cambridge, 2010).
- [38] F. J. Dyson, The Radiation Theories of Tomonaga, Schwinger, and Feynman, *Phys. Rev.* **75**, 486 (1949).
- [39] T. J. Green, J. Sastrawan, H. Uys, and M. J. Biercuk, Arbitrary quantum control of qubits in the presence of universal noise, *New J. Phys.* **15**, 095004 (2013).
- [40] See Supplemental Material for more details.
- [41] N. Khaneja, T. Reiss, C. Kehlet, T. Schulte-Herbrüggen, and S. J. Glaser, Optimal control of coupled spin dynamics: design of nmr pulse sequences by gradient ascent algorithms, *J. Magn. Reson.* **172**, 296 (2005).
- [42] A. J. Leggett, S. Chakravarty, A. T. Dorsey, M. P. A. Fisher, A. Garg, and W. Zwerger, Dynamics of the dissipative two-state system, *Rev. Mod. Phys.* **59**, 1 (1987).
- [43] M. Bando, T. Ichikawa, Y. Kondo, and M. Nakahara, Concatenated composite pulses compensating simultaneous systematic errors, *J. Phys. Soc. Japan* **82**, 014004 (2012).
- [44] F. Yan, S. Gustavsson, J. Bylander, X. Jin, F. Yoshihara, D. G. Cory, Y. Nakamura, T. P. Orlando, and W. D. Oliver, Rotating-frame relaxation as a noise spectrum analyser of a superconducting qubit undergoing driven evolution, *Nat. Commun.* **4**, 1 (2013).
- [45] J. Jeener, Superoperators in magnetic resonance, *Adv. Magn. Reson.* **10**, 1 (1982).
- [46] G. Wolfowicz, F. J. Heremans, C. P. Anderson, S. Kanai, H. Seo, A. Gali, G. Galli, and D. D. Awschalom, Quantum guidelines for solid-state spin defects, *Nat. Rev. Mater.* **6**, 906 (2021).
- [47] H. Haas, D. Pizzuoli, F. Zhang, and D. G. Cory, Engineering effective Hamiltonians, *New J. Phys.* **21**, 103011 (2019).
- [48] E. Barnes, Analytically solvable two-level quantum systems and landau-zener interferometry, *Phys. Rev. A* **88**, 013818 (2013).
- [49] E. Barnes and S. Das Sarma, Analytically Solvable Driven Time-Dependent Two-Level Quantum Systems, *Phys. Rev. Lett.* **109**, 060401 (2012).
- [50] P. Titum, K. Schultz, A. Seif, G. Quiroz, and B. Clader, Optimal control for quantum detectors, *Npj Quantum Inf.* **7**, 1 (2021).
- [51] N. Bar-Gill, L. M. Pham, C. Belthangady, D. Le Sage, P. Cappellaro, J. Maze, M. D. Lukin, A. Yacoby, and R. Walsworth, Suppression of spin-bath dynamics for improved coherence of multi-spin-qubit systems, *Nat. Commun.* **3**, 1 (2012).
- [52] L. Hall, P. Kehayias, D. A. Simpson, A. Jarmola, A. Stacey, D. Budker, and L. C. L. Hollenberg, Detection of nanoscale electron spin resonance spectra demonstrated using nitrogen-vacancy centre probes in diamond, *Nat. Commun.* **7**, 10211 (2015).
- [53] K. W. Chan, W. Huang, C. H. Yang, J. C. C. Hwang, B. Hensen, T. Tanttu, F. E. Hudson, K. M. Itoh, A. Laucht, A. Morello, and A. S. Dzurak, Assessment of a Silicon Quantum Dot Spin Qubit Environment via Noise Spectroscopy, *Phys. Rev. Applied* **10**, 044017 (2018).

## Supplementary Material

### INVERSE GEOMETRIC OPTIMIZATION FOR SINGLE-QUBIT QUANTUM SYSTEM

#### Derivation of Eq. (2) of the Main Text: Evolution Parameterization

An arbitrary single-qubit noise-free evolution can be parameterized by

$$U = \begin{bmatrix} \cos(\theta/2)e^{-i\varphi/2}e^{-i\gamma/2} & -\sin(\theta/2)e^{-i\varphi/2}e^{i\gamma/2} \\ \sin(\theta/2)e^{i\varphi/2}e^{-i\gamma/2} & \cos(\theta/2)e^{i\varphi/2}e^{i\gamma/2} \end{bmatrix}.$$

Using this, the Schrödinger equation can be rewritten as

$$\begin{bmatrix} \dot{U}_{11} & \dot{U}_{12} \\ \dot{U}_{21} & \dot{U}_{22} \end{bmatrix} = \begin{bmatrix} 0 & (-iu_x - u_y)/2 \\ (-iu_x + u_y)/2 & 0 \end{bmatrix} \begin{bmatrix} U_{11} & U_{12} \\ U_{21} & U_{22} \end{bmatrix}$$

which is

$$-\frac{\dot{\theta}}{2} \sin(\theta/2) - \frac{i\dot{\varphi}}{2} \cos(\theta/2) - \frac{i\dot{\gamma}}{2} \cos(\theta/2) = \frac{1}{2}(-iu_x - u_y) \sin(\theta/2)e^{i\varphi}, \quad (\text{S.1a})$$

$$-\frac{\dot{\theta}}{2} \cos(\theta/2) + \frac{i\dot{\varphi}}{2} \sin(\theta/2) - \frac{i\dot{\gamma}}{2} \sin(\theta/2) = \frac{1}{2}(-iu_x - u_y) \cos(\theta/2)e^{i\varphi}, \quad (\text{S.1b})$$

$$\frac{\dot{\theta}}{2} \cos(\theta/2) + \frac{i\dot{\varphi}}{2} \sin(\theta/2) - \frac{i\dot{\gamma}}{2} \sin(\theta/2) = \frac{1}{2}(-iu_x + u_y) \cos(\theta/2)e^{-i\varphi}, \quad (\text{S.1c})$$

$$-\frac{\dot{\theta}}{2} \sin(\theta/2) + \frac{i\dot{\varphi}}{2} \cos(\theta/2) + \frac{i\dot{\gamma}}{2} \cos(\theta/2) = \frac{1}{2}(iu_x - u_y) \sin(\theta/2)e^{-i\varphi}. \quad (\text{S.1d})$$

From these equations, we can obtain

$$\dot{\theta} = -u_x \sin \varphi + u_y \cos \varphi = \Omega \sin(\phi - \varphi), \quad (\text{S.2a})$$

$$\dot{\varphi} = -(u_x \cos \varphi + u_y \sin \varphi) \cot(\theta) = -\Omega \cos(\phi - \varphi) \cot \theta, \quad (\text{S.2b})$$

$$\dot{\gamma} = (u_x \cos \varphi + u_y \sin \varphi) / \sin(\theta) = \Omega \cos(\phi - \varphi) / \sin \theta. \quad (\text{S.2c})$$

Once a robust evolution trajectory is obtained, we can determine the control fields by

$$\Omega(t) = \sqrt{\dot{\theta}^2 + \dot{\gamma}^2 \sin^2 \theta}, \phi(t) = \arcsin(\dot{\theta}/\Omega) + \varphi. \quad (\text{S.3})$$

### Derivation of Eq. (3) of the Main Text: Average Gate Infidelity

For one realization of noise  $\epsilon_a(t)$  and  $\epsilon_d(t)$ , the real gate fidelity is

$$F = \left| \text{Tr} \left( \bar{U}^\dagger U_{\epsilon_a, \epsilon_d}(T) \right) \right|^2 / 4 = |\text{Tr} (U_{\text{tog}}(T))|^2 / 4. \quad (\text{S.4})$$

It is convenient to write  $U_{\text{tog}}(T) = \exp\{-i \sum_{\mu=a,d} \int_0^T \epsilon_\mu(t) \tilde{E}_\mu(t) dt\} \equiv e^{-i\mathbf{a} \cdot \boldsymbol{\sigma} / 2} = \mathbf{1} \cos(a/2) - i \sin(a/2) \mathbf{a} \cdot \boldsymbol{\sigma} / a$ , where  $\boldsymbol{\sigma} = (\sigma_x, \sigma_y, \sigma_z)$ , thus  $F = [1 + \cos(a)]/2$ . For the first-order approximation, we obtain  $F \approx 1 - a^2/4$ . Take the ensemble average of the noise, we get the average gate infidelity

$$\begin{aligned} \mathcal{F}_{\text{avg}} &= 1 - \langle F \rangle \approx \sum_{\mu=a,d} \left[ \int_0^T dt_1 \int_0^T dt_2 \epsilon_\mu(t_1) \epsilon_\mu(t_2) \sum_{\alpha=x,y,z} \text{Tr}[\tilde{E}_{\mu,\alpha}(t_1) \sigma_\alpha / 2] \text{Tr}[\tilde{E}_{\mu,\alpha}(t_2) \sigma_\alpha / 2] \right] \\ &= \frac{1}{2\pi} \sum_{\substack{\mu=a,d \\ \alpha=x,y,z}} \int_{-\infty}^{\infty} \frac{d\omega}{\omega^2} S_\mu(\omega) |R_{\mu,\alpha}(\omega)|^2. \end{aligned} \quad (\text{S.5})$$

where  $R_{\mu,\alpha}(\omega) = -i\omega \int_0^T dt \text{Tr}[\tilde{E}_{\mu,\alpha}(t) \sigma_\alpha / 2] e^{i\omega t}$ .

### Derivation of Eq. (4) of the Main Text: Average State Transfer Infidelity

For one realization of noise  $\epsilon_a(t)$  and  $\epsilon_d(t)$ , the real state fidelity is

$$\begin{aligned} F &= |\langle \bar{\psi} | U_{\epsilon_a, \epsilon_d}(T) | 0 \rangle|^2 = |\langle 0 | U_{\text{tog}}(T) | 0 \rangle|^2 \\ &= |\langle 0 | (\mathbf{1} - \sum_{\mu=a,d} [i \int_0^T dt_1 \epsilon_\mu(t_1) \tilde{E}_\mu(t_1) + \int_0^T dt_1 \int_0^{t_1} dt_2 \epsilon_\mu(t_1) \epsilon_\mu(t_2) \tilde{E}_\mu(t_1) \tilde{E}_\mu(t_2) + \dots]) | 0 \rangle|^2 \\ &\approx 1 + \sum_{\mu=a,d} \int_0^T dt_1 \int_0^T dt_2 \epsilon_\mu(t_1) \epsilon_\mu(t_2) \langle 0 | \tilde{E}_\mu(t_1) | 0 \rangle \langle 0 | \tilde{E}_\mu(t_2) | 0 \rangle^* \\ &\quad - \sum_{\mu=a,d} \int_0^T dt_1 \int_0^{t_1} dt_2 \epsilon_\mu(t_1) \epsilon_\mu(t_2) \langle 0 | \tilde{E}_\mu(t_1) \tilde{E}_\mu(t_2) | 0 \rangle - \sum_{\mu=a,d} \int_0^T dt_1 \int_0^{t_1} dt_2 \epsilon_\mu(t_1) \epsilon_\mu(t_2) \langle 0 | \tilde{E}_\mu(t_1) \tilde{E}_\mu(t_2) | 0 \rangle^*, \end{aligned} \quad (\text{S.6})$$

where we omit the cross terms containing  $\epsilon_{\mu_1}(t_1)\epsilon_{\mu_2}(t_2)$  with  $\mu_1 \neq \mu_2$ . Insert  $|0\rangle\langle 0| + |1\rangle\langle 1|$  into the expression, then

$$F \approx 1 - \sum_{\mu=a,d} \int_0^T dt_1 \int_0^T dt_2 \epsilon_{\mu}(t_1)\epsilon_{\mu}(t_2) \langle 0|\tilde{E}_{\mu}(t_1)|1\rangle\langle 1|\tilde{E}_{\mu}(t_2)|0\rangle. \quad (\text{S.7})$$

Thus the average state infidelity is

$$\mathcal{F}_{\text{avg}} = 1 - \langle F \rangle \approx \sum_{\substack{\mu=a,d \\ \alpha=x,y,z}} \frac{1}{2\pi} \int_{-\infty}^{\infty} \frac{d\omega}{\omega^2} S_{\mu}(\omega) |P_{\mu,\alpha}(\omega)|^2, \quad (\text{S.8})$$

where  $P_{\mu,\alpha} = -i\omega \int_0^T dt \langle 0|\tilde{E}_{\mu,\alpha}(t)|1\rangle e^{i\omega t}$ .

### Gradient-based Optimization

To search robust trajectory, we apply gradient-based optimization. In our optimization, we discretize  $\theta(t)$  and  $\gamma(t)$  as  $M$ -slice sequences  $\theta[1], \dots, \theta[M]$  and  $\gamma[1], \dots, \gamma[M]$ , respectively, with the time length of each slice  $\tau = T/M$ . For quantum gate, the derivative of the average gate infidelity function reads

$$\begin{aligned} \frac{\partial \mathcal{F}_{\text{avg}}}{\partial \chi[m]} &= \sum_{\substack{\mu=a,d \\ \alpha=x,y,z}} \frac{1}{2\pi} \int_{-\infty}^{\infty} \frac{d\omega}{\omega^2} S_{\mu}(\omega) \text{Re} \left\{ \frac{\partial R_{\mu,\alpha}(\omega)}{\partial \chi[m]} R_{\mu,\alpha}^*(\omega) \right\} \\ &= \sum_{\substack{\mu=a,d \\ \alpha=x,y,z}} \frac{1}{2\pi} \int_{-\infty}^{\infty} \frac{d\omega}{\omega^2} S_{\mu}(\omega) \text{Re} \left\{ -i\omega\tau e^{i\omega m\tau} \frac{\partial \text{Tr}[\tilde{E}_{\mu,\alpha}[m] \frac{\sigma_{\alpha}}{2}]}{\partial \chi[m]} R_{\mu,\alpha}^*(\omega) \right\}, \chi = \theta, \gamma. \end{aligned} \quad (\text{S.9})$$

Similarly, for quantum state transfer, the derivative of the average state infidelity function reads

$$\begin{aligned} \frac{\partial \mathcal{F}_{\text{avg}}}{\partial \chi[m]} &= \sum_{\substack{\mu=a,d \\ \alpha=x,y,z}} \frac{1}{2\pi} \int_{-\infty}^{\infty} \frac{d\omega}{\omega^2} S_{\mu}(\omega) \text{Re} \left\{ \frac{\partial P_{\mu,\alpha}(\omega)}{\partial \chi[m]} P_{\mu,\alpha}^*(\omega) \right\} \\ &= \sum_{\substack{\mu=a,d \\ \alpha=x,y,z}} \frac{1}{2\pi} \int_{-\infty}^{\infty} \frac{d\omega}{\omega^2} S_{\mu}(\omega) \text{Re} \left\{ -i\omega\tau e^{i\omega m\tau} \frac{\partial \text{Tr}[\tilde{E}_{\mu,\alpha}[m] |1\rangle\langle 0|]}{\partial \chi[m]} P_{\mu,\alpha}^*(\omega) \right\}, \chi = \theta, \gamma. \end{aligned} \quad (\text{S.10})$$

The above gradients are then used to update the trajectory by  $\chi[m] \leftarrow \chi[m] + l \frac{\partial \mathcal{F}_{\text{avg}}}{\partial \chi[m]}$ , where  $l$  is appropriate step size.

We test our robust control method for realizing a  $\pi$  rotational gate or state transfer from  $|0\rangle$  to  $|1\rangle$  subject to various types of time-dependent noise, as shown in Figs. S1-S2 and Figs. S3-S4, respectively. For detuning noise, we compare the performance between three sequences, namely primitive, CORPSE and ROC pulses, see the results in Figs. S1-S4(a<sub>1</sub>)–(a<sub>3</sub>), (b<sub>1</sub>)–(b<sub>3</sub>), (c<sub>1</sub>)–(c<sub>3</sub>). Specifically, we consider (i) ohmic spectrum with sharp cut-offs, i.e.,  $S_d(\omega) \propto \omega, \omega \in [\omega_{lc}, \omega_{uc}]$ , which describes a spin suffering bosonic environment [42]; (ii) single Lorentzian spectrum  $S_d(\omega) \propto 1/(\lambda^2 + (\omega - \omega_0)^2)$  or multiple Lorentzian spectrum  $S_d(\omega) \propto \sum_k A_k/(\lambda_k^2 + (\omega - \omega_{0,k})^2)$ , which captures the solid-state spin environment of a spin bath as measured in, e.g., Refs. [51, 52]. For amplitude noise, we compare the performance between primitive, BB1 and ROC pulses, as shown in Figs. S1-S4(d<sub>1</sub>)–(d<sub>3</sub>), (e<sub>1</sub>)–(e<sub>3</sub>). Here we examine (i) a noise model corresponding to a strong and narrow Gaussian peak added on top of a broad  $1/f^{\kappa}$  background with a roll-off to white noise, i.e.,  $S_a(\omega) \propto A \exp[-(\omega - \omega_0)^2/(2\sigma^2)] + B/\omega^{\kappa}, \omega < \omega_{wc}; S_a(\omega) = \text{const.}, \omega \geq \omega_{wc}$ . This type of noise spectrum was observed, for example, in a silicon quantum dot spin qubit due to the imperfect control apparatus [53]. (ii) several Lorentzian peaks added on top of a broad  $1/f^{\kappa}$  background  $S_a(\omega) \propto \sum_k A_k/(\lambda_k^2 + (\omega - \omega_{0,k})^2) + B/\omega^{\kappa}$ , which describes the random fluctuations in superconducting flux terms [44]. For simultaneous detuning noise and amplitude noise, for simplicity, we choose both of the noise spectrums as a single Lorentzian peak added on top of a broad  $1/f$  background, i.e.,  $S_{\mu}(\omega) \propto A/(\lambda^2 + (\omega - \omega_0)^2) + B/\omega$ . We compare the performance between primitive, reduced CinBB and ROC pulses. Reduced CinBB [43] is a concatenated composite pulse for suppressing both of the detuning and amplitude noises. Results are summarized in Figs. S1-S4(f<sub>1</sub>)–(f<sub>3</sub>). We also list explicitly the parameters of the noise power density spectrums and the tested control sequences in Table. I. All the simulations reveal that our ROC method find high-quality, smooth and low-power robust pulses for resisting various realistic time-dependent noises. In the main text, we demonstrate several typical results to show the effectiveness of our robust control method.



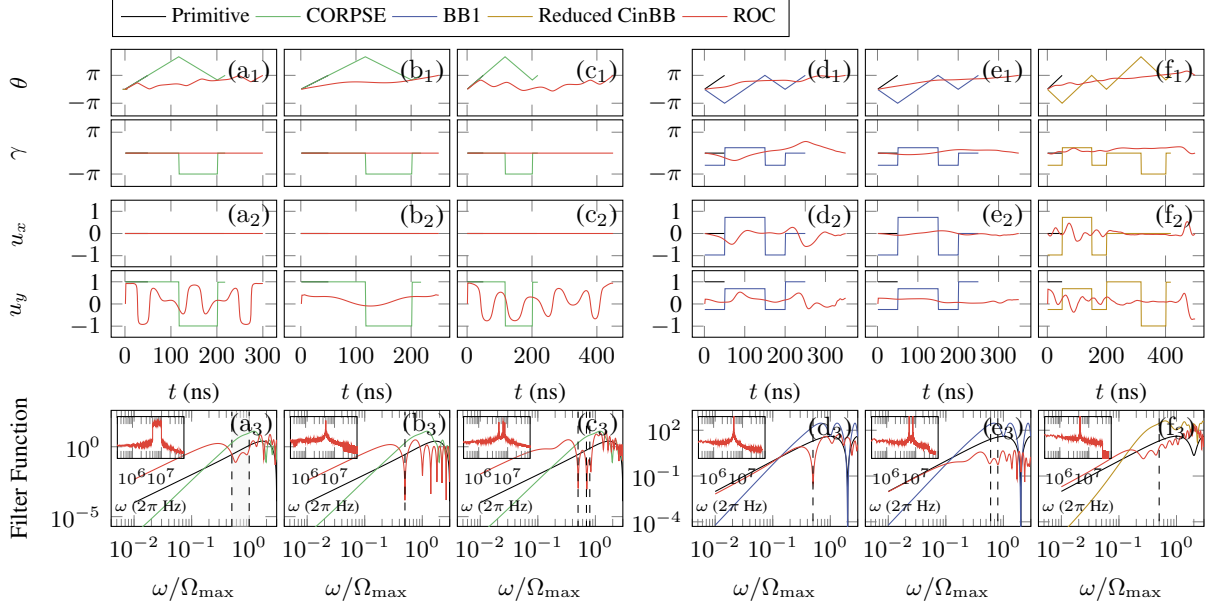


FIG. S1. Geometric trajectories, control waveforms (in the unit of  $\Omega_{\max}$ ), FFs and noise spectrums of different sequences for realizing a  $\pi$  rotation gate subject to high-frequency time-dependent (a<sub>1</sub>)–(a<sub>3</sub>), (b<sub>1</sub>)–(b<sub>3</sub>), (c<sub>1</sub>)–(c<sub>3</sub>) detuning noise, (d<sub>1</sub>)–(d<sub>3</sub>), (e<sub>1</sub>)–(e<sub>3</sub>) amplitude noise, or (f<sub>1</sub>)–(f<sub>3</sub>) both. For detuning noise, the strength is  $\sqrt{\langle \epsilon_d^2(0) \rangle} = 0.03\Omega_{\max}$  with  $\Omega_{\max}/(2\pi) = 10^7$  Hz, and the noise spectrums are ohmic (insert in (a<sub>3</sub>)), single Lorentzian (insert in (b<sub>3</sub>),  $\lambda = 100$  Hz), or multiple Lorentzian (insert in (c<sub>3</sub>),  $\lambda_1 = \lambda_2 = \lambda_3 = 100$  Hz,  $A_1 = 0.8, A_2 = 1.5, A_3 = 0.6$ ), respectively. For amplitude noise, the strength is  $\sqrt{\langle \epsilon_a^2(0) \rangle} = 0.03$ , and the noise spectrums are a Gaussian peak added on top of  $1/f$  background with a roll-off to white noise (insert in (d<sub>3</sub>),  $\sigma = 5000$  Hz,  $\kappa = 1, A = 1, B = 0.05, \omega_{wc} = \Omega_{\max}$ ), or two Lorentzian peaks added on top of  $1/f$  background (insert in (e<sub>3</sub>),  $\lambda_1 = \lambda_2 = 100$  Hz,  $\kappa = 1, A_1 = A_2 = 1, B = 0.05$ ), respectively. For simultaneous detuning noise and amplitude noise, the noise spectrums are both chosen as a single Lorentzian peak added on top of  $1/f$  background (insert in (f<sub>3</sub>),  $\lambda = 100$  Hz,  $\kappa = 1, A = 1, B = 0.05$ ) with the same strengths as above.

Noise feature		Primitive			CORPSE/BB1/CinBB			ROC			
Noise spectrum type	$[\omega_{lc}, \omega_{uc}] / \omega_{0,k} (*\Omega_{\max})$	Pulse Length (* $T_p$ )	Gate Infidelity	State Infidelity	Pulse Length (* $T_p$ )	Gate Infidelity	State Infidelity	Pulse Length (* $T_p$ )	Gate Infidelity	Pulse Length (* $T_p$ )	State Infidelity
Ohmic	[0.5, 1.0]	1	$1 * 10^{-3}$	$6 * 10^{-4}$	4.3	$9 * 10^{-3}$	$2 * 10^{-3}$	6	$4 * 10^{-4}$	5	$1 * 10^{-5}$
	[0.2, 0.4]	1	$1 * 10^{-3}$	$9 * 10^{-4}$	4.3	$3 * 10^{-3}$	$1 * 10^{-3}$	8	$5 * 10^{-4}$	6	$1 * 10^{-5}$
Single Lorentzian	0.5	1	$1 * 10^{-3}$	$7 * 10^{-4}$	4.3	$6 * 10^{-3}$	$2 * 10^{-3}$	5	$3 * 10^{-6}$	4	$2 * 10^{-5}$
	0.1	1	$9 * 10^{-4}$	$9 * 10^{-4}$	4.3	$4 * 10^{-4}$	$1 * 10^{-4}$	7	$3 * 10^{-5}$	4	$2 * 10^{-5}$
Multiple Lorentzian	0.5, 0.7, 0.8	1	$1 * 10^{-3}$	$6 * 10^{-4}$	4.3	$9 * 10^{-3}$	$8 * 10^{-4}$	9	$5 * 10^{-5}$	7	$4 * 10^{-6}$
	0.1, 0.3, 0.4	1	$9 * 10^{-4}$	$8 * 10^{-4}$	4.3	$2 * 10^{-3}$	$9 * 10^{-4}$	14	$1 * 10^{-4}$	10	$3 * 10^{-5}$
Gaussian+ $1/f$ +white noise roll-off	0.5	1	$2 * 10^{-3}$	$2 * 10^{-3}$	5	$1 * 10^{-2}$	$1 * 10^{-2}$	7	$3 * 10^{-5}$	7	$2 * 10^{-5}$
	0.2	1	$2 * 10^{-3}$	$2 * 10^{-3}$	5	$4 * 10^{-3}$	$4 * 10^{-3}$	8	$3 * 10^{-5}$	8	$7 * 10^{-5}$
Multiple Lorentzian + $1/f$	0.6, 0.8	1	$2 * 10^{-3}$	$2 * 10^{-3}$	5	$1 * 10^{-2}$	$1 * 10^{-2}$	7	$4 * 10^{-5}$	7	$6 * 10^{-5}$
	0.2, 0.4	1	$2 * 10^{-3}$	$2 * 10^{-3}$	5	$8 * 10^{-3}$	$9 * 10^{-3}$	9	$6 * 10^{-5}$	9	$9 * 10^{-5}$
Both: Lorentzian+ $1/f$	0.5	1	$3 * 10^{-3}$	$3 * 10^{-3}$	8.3	$2 * 10^{-2}$	$2 * 10^{-2}$	10	$3 * 10^{-4}$	8	$3 * 10^{-4}$
	0.3	1	$3 * 10^{-3}$	$3 * 10^{-3}$	8.3	$3 * 10^{-2}$	$4 * 10^{-2}$	11	$3 * 10^{-4}$	11	$2 * 10^{-4}$

TABLE I. Noise spectrum features and sequence parameters for realizing a  $\pi$  rotational gate or state transfer from  $|0\rangle$  to  $|1\rangle$  subject to time-dependent detuning noise (the first sub table), amplitude noise (the second sub table) or both (the third sub table), respectively, where  $\Omega_{\max}$  is the maximum rabi frequency,  $T_p$  represents the length of primitive sequence.

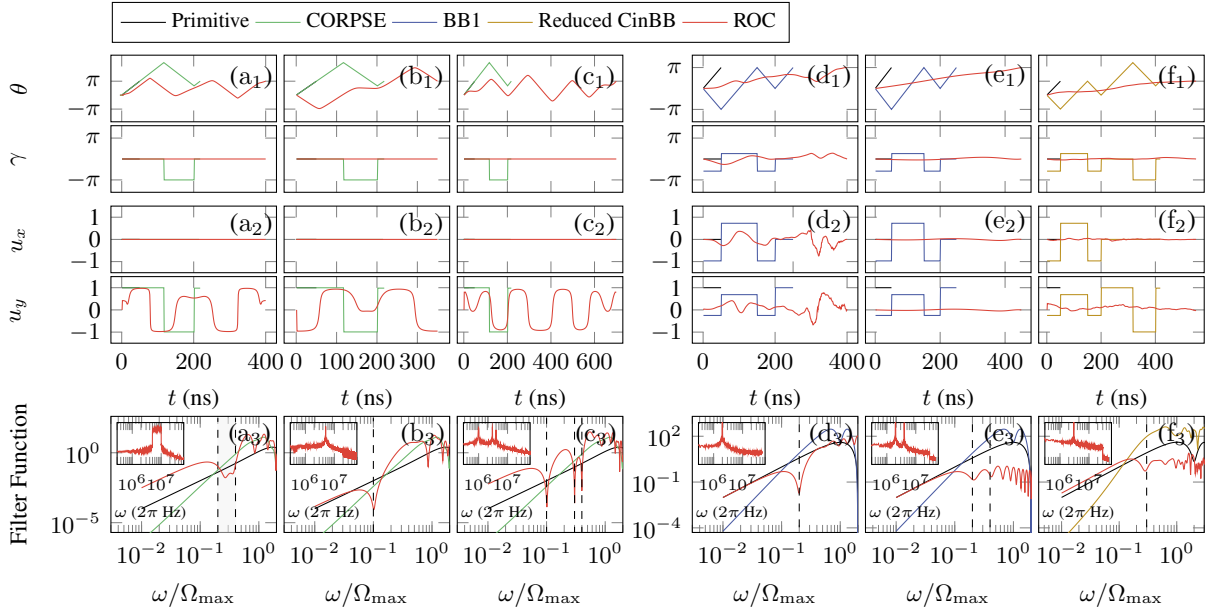


FIG. S2. Geometric trajectories, control waveforms, FFs and noise spectrums of different sequences for realizing a  $\pi$  rotation gate subject to low-frequency time-dependent (a<sub>1</sub>)–(a<sub>3</sub>), (b<sub>1</sub>)–(b<sub>3</sub>), (c<sub>1</sub>)–(c<sub>3</sub>) detuning noise, (d<sub>1</sub>)–(d<sub>3</sub>), (e<sub>1</sub>)–(e<sub>3</sub>) amplitude noise, or (f<sub>1</sub>)–(f<sub>3</sub>) both. For detuning noise, the noise spectrums are ohmic (insert in (a<sub>3</sub>)), single Lorentzian (insert in (b<sub>3</sub>),  $\lambda = 100$  Hz), or multiple Lorentzian (insert in (c<sub>3</sub>)), respectively. For amplitude noise, the noise spectrums are a Gaussian peak added on top of  $1/f$  background with a roll-off to white noise (insert in (d<sub>3</sub>)), or two Lorentzian peaks added on top of  $1/f$  background (insert in (e<sub>3</sub>)), respectively. For simultaneous detuning noise and amplitude noise, the noise spectrums are both chosen as a single Lorentzian peak added on top of  $1/f$  background (insert in (f<sub>3</sub>)) with the same strengths as above. All the spectrum and control pulse parameters are the same with above case.

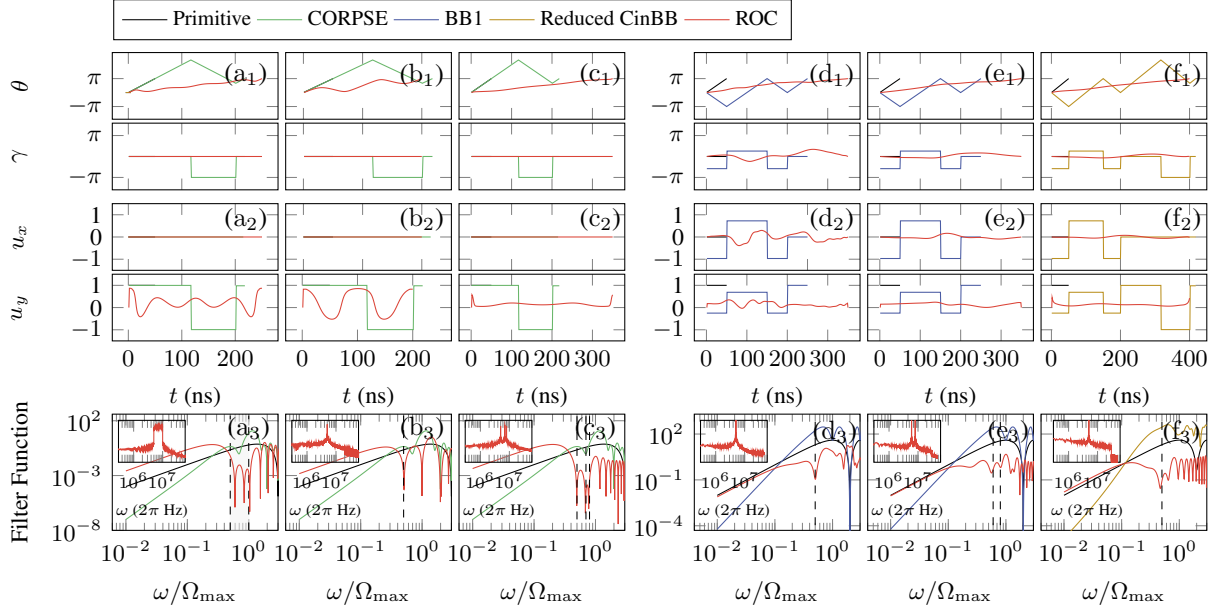


FIG. S3. Geometric trajectories, control waveforms, FFs and noise spectrums of different sequences for realizing state transfer from  $|0\rangle$  to  $|1\rangle$  subject to high-frequency time-dependent (a<sub>1</sub>)–(a<sub>3</sub>), (b<sub>1</sub>)–(b<sub>3</sub>), (c<sub>1</sub>)–(c<sub>3</sub>) detuning noise, (d<sub>1</sub>)–(d<sub>3</sub>), (e<sub>1</sub>)–(e<sub>3</sub>) amplitude noise, or (f<sub>1</sub>)–(f<sub>3</sub>) both. For detuning noise, the noise spectrums are ohmic (insert in (a<sub>3</sub>)), single Lorentzian (insert in (b<sub>3</sub>)), or multiple Lorentzian (insert in (c<sub>3</sub>)), respectively. For amplitude noise, the noise spectrums are a Gaussian peak added on top of  $1/f$  background with a roll-off to white noise (insert in (d<sub>3</sub>)), or two Lorentzian peaks added on top of  $1/f$  background (insert in (e<sub>3</sub>)), respectively. For simultaneous detuning noise and amplitude noise, the noise spectrums are both chosen as a single Lorentzian peak added on top of  $1/f$  background (insert in (f<sub>3</sub>)) with the same strengths as above. All the spectrum and control pulse parameters are the same with that in quantum gate case.

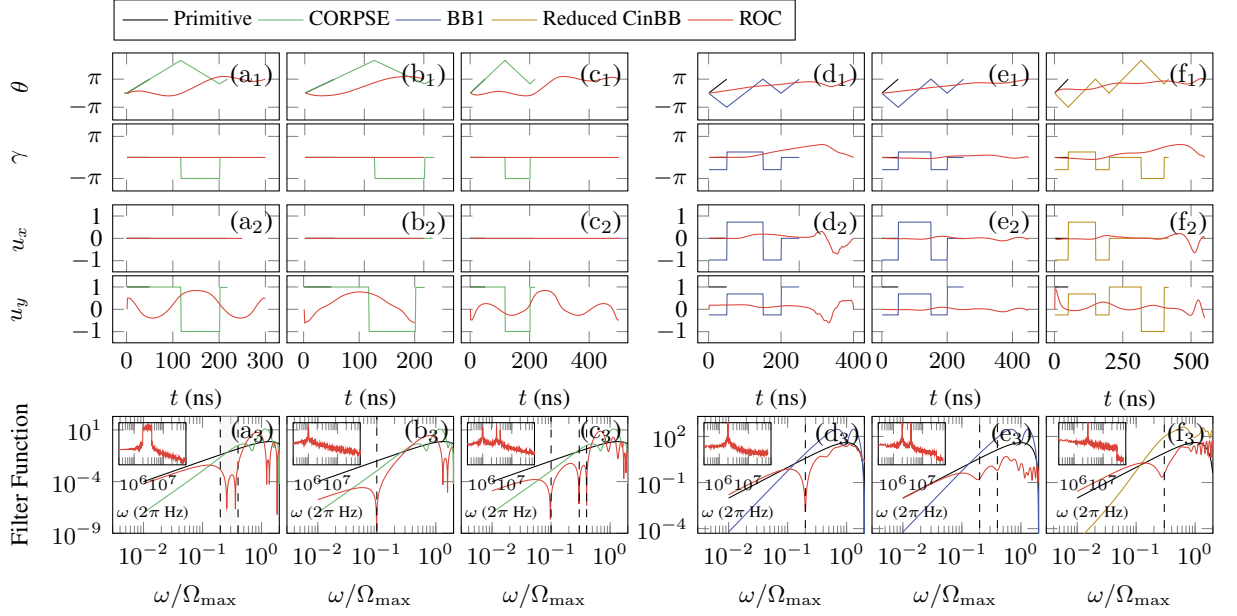


FIG. S4. Geometric trajectories, control waveforms, FFs and noise spectrums of different sequences for realizing state transfer from  $|0\rangle$  to  $|1\rangle$  subject to low-frequency time-dependent (a<sub>1</sub>)–(a<sub>3</sub>), (b<sub>1</sub>)–(b<sub>3</sub>), (c<sub>1</sub>)–(c<sub>3</sub>) detuning noise, (d<sub>1</sub>)–(d<sub>3</sub>), (e<sub>1</sub>)–(e<sub>3</sub>) amplitude noise, or (f<sub>1</sub>)–(f<sub>3</sub>) both. For detuning noise, the noise spectrums are ohmic (insert in (a<sub>3</sub>)), single Lorentzian (insert in (b<sub>3</sub>)), or multiple Lorentzian (insert in (c<sub>3</sub>)), respectively. For amplitude noise, the noise spectrums are a Gaussian peak added on top of  $1/f$  background with a roll-off to white noise (insert in (d<sub>3</sub>)), or two Lorentzian peaks added on top of  $1/f$  background (insert in (e<sub>3</sub>)), respectively. For simultaneous detuning noise and amplitude noise, the noise spectrums are both chosen as a single Lorentzian peak added on top of  $1/f$  background (insert in (f<sub>3</sub>)) with the same strengths as above. All the spectrum and control pulse parameters are the same with that in quantum gate case.

## INVERSE GEOMETRIC OPTIMIZATION FOR TWO-LEVEL OPEN QUANTUM SYSTEM

### Evolution Parameterization

For an isolated spin-1/2 ensemble, the density matrix can be conventionally expressed as  $\rho = \mathbb{1}/2 + x_1\sigma_x + x_2\sigma_y + x_3\sigma_z$ . When undergoing both transverse and longitudinal relaxation, and under Markovian approximation, the system dynamics under controls  $u_x = \Omega(t) \cos(\phi(t))$ ,  $u_y = \Omega(t) \sin(\phi(t))$  can be described by the Bloch equations

$$\dot{x} = (H_0(t) + \gamma_1 R_{T_1} + \gamma_2 R_{T_2})x, \quad (\text{S.11})$$

where  $x = (1/2, x_1, x_2, x_3)^T$ ,  $\gamma_{1,2} = 1/T_{1,2}$  are relaxation parameters and

$$H_0(t) = \begin{pmatrix} 0 & 0 & 0 & 0 \\ 0 & 0 & -\Omega_0 & u_y \\ 0 & \Omega_0 & 0 & -u_x \\ 0 & -u_y & u_x & 0 \end{pmatrix}, R_{T_1} = \begin{pmatrix} 0 & 0 & 0 & 0 \\ 0 & 0 & 0 & 0 \\ 0 & 0 & 0 & 0 \\ 2M_0 & 0 & 0 & -1 \end{pmatrix}, R_{T_2} = \begin{pmatrix} 0 & 0 & 0 & 0 \\ 0 & -1 & 0 & 0 \\ 0 & 0 & -1 & 0 \\ 0 & 0 & 0 & 0 \end{pmatrix}. \quad (\text{S.12})$$

For simplicity, we set the off-resonance frequency  $\Omega_0 = 0$  and the equilibrium state polarization  $M_0 = 1$ .

To apply inverse geometric optimization, we introduce the three-dimensional rotations

$$R_z(\delta) = \begin{pmatrix} \cos \delta & -\sin \delta & 0 \\ \sin \delta & \cos \delta & 0 \\ 0 & 0 & 1 \end{pmatrix}, R_y(\eta) = \begin{pmatrix} \cos \eta & 0 & \sin \eta \\ 0 & 1 & 0 \\ -\sin \eta & 0 & \cos \eta \end{pmatrix}, R_z(\xi) = \begin{pmatrix} \cos \xi & -\sin \xi & 0 \\ \sin \xi & \cos \xi & 0 \\ 0 & 0 & 1 \end{pmatrix}. \quad (\text{S.13})$$

As such, the noise-free evolution of two-level open quantum system can be parameterized by

$$\begin{aligned} V_0(t) &= \begin{pmatrix} 1 & 0 \\ 0 & R_z(\delta)R_y(\eta)R_z(\xi) \end{pmatrix} \\ &= \begin{pmatrix} 1 & 0 & 0 & 0 \\ 0 & \cos(\delta)\cos(\eta)\cos(\xi) - \sin(\delta)\sin(\xi) & -\sin(\delta)\cos(\xi) - \cos(\delta)\cos(\eta)\sin(\xi) & \cos(\delta)\sin(\eta) \\ 0 & \sin(\delta)\cos(\eta)\cos(\xi) + \cos(\delta)\sin(\xi) & \cos(\delta)\cos(\xi) - \sin(\delta)\cos(\eta)\sin(\xi) & \sin(\delta)\sin(\eta) \\ 0 & -\sin(\eta)\cos(\xi) & \sin(\eta)\sin(\xi) & \cos(\eta) \end{pmatrix}, \end{aligned} \quad (\text{S.14})$$

thus the Bloch equation becomes

$$\dot{V}_0(t) = H_0(t)V_0(t), H_0(t) = \begin{pmatrix} 0 & 0 & 0 & 0 \\ 0 & 0 & 0 & u_y \\ 0 & 0 & 0 & -u_x \\ 0 & -u_y & u_x & 0 \end{pmatrix}. \quad (\text{S.15})$$

This then gives

$$\dot{\xi} = (u_x \cos \delta + u_y \sin \delta) / \sin \eta = \Omega \cos(\phi - \delta) / \sin \eta, \quad (\text{S.16a})$$

$$\dot{\eta} = u_y \cos \delta - u_x \sin \delta = \Omega \sin(\phi - \delta), \quad (\text{S.16b})$$

$$\dot{\delta} = -(u_x \cos \delta + u_y \sin \delta) / \tan \eta = -\Omega \cos(\phi - \delta) / \tan \eta. \quad (\text{S.16c})$$

Once a robust evolution trajectory is obtained, we can determine the control fields by

$$\Omega(t) = \sqrt{\dot{\eta}^2 + \dot{\xi}^2 \sin^2 \eta}, \phi(t) = \arcsin(\dot{\eta} / \Omega) + \delta. \quad (\text{S.17})$$

### State Transfer Infidelity

To characterize the distance between the actual state  $V_{T_1, T_2}(T)x(0)$  and the target state  $\bar{x}$ , we define

$$\begin{aligned} \mathcal{F} &= |\bar{x} - V_{T_1, T_2}(T)x(0)|^2 = [\bar{x} - V_{T_1, T_2}(T)x(0)]^T [\bar{x} - V_{T_1, T_2}(T)x(0)] \\ &= [\bar{x} - V_0(T)V_{\text{tog}}(T)x(0)]^T [\bar{x} - V_0(T)V_{\text{tog}}(T)x(0)] \\ &\approx \left[ V_0(T)x(0) - V_0(T)(\mathbb{1} + \sum_{k=1,2} \int_0^T dt \gamma_k \tilde{R}_{T_k}(t))x(0) \right]^T \left[ V_0(T)x(0) - V_0(T)(\mathbb{1} + \sum_{k=1,2} \int_0^T dt \gamma_k \tilde{R}_{T_k}(t))x(0) \right] \\ &= \left[ \sum_{k=1,2} \int_0^T dt \gamma_k \tilde{R}_{T_k}(t)x(0) \right]^T \left[ \sum_{j=1,2} \int_0^T dt \gamma_j \tilde{R}_{T_j}(t)x(0) \right] \\ &= \sum_{k=1,2} \left[ \int_0^T dt \gamma_k \tilde{R}_{T_k}(t)x(0) \right]^T \left[ \int_0^T dt \gamma_k \tilde{R}_{T_k}(t)x(0) \right], \end{aligned} \quad (\text{S.18})$$

where one should notice that  $[\tilde{R}_{T_k}x(0)]^T [\tilde{R}_{T_j}x(0)] = 0$  when  $k \neq j$ .